Subtle escaping modes and subset of patterns from a nonhyperbolic chaotic attractor

Zhen Chen* and Xianbin Liu†

State Key Laboratory of Mechanics and Control for Mechanical Structures, College of Aerospace Engineering, Nanjing University of Aeronautics and Astronautics, 29 Yudao Street, Nanjing 210016, People's Republic of China

(Received 24 August 2016; published 17 January 2017)

Noise-induced escape from the domain of attraction of a nonhyperbolic chaotic attractor in a periodically excited nonlinear oscillator is further investigated. Deviations are found to be amplified at the primary homoclinic tangency from which the optimal force begins to fluctuate dramatically. Escaping trajectories turn out to possess several modes to pass through the saddle cycle on the basin boundary, and each mode corresponds to a certain type of value of the action plot, respectively. A subset of the pattern of fluctuational paths from the chaotic attractor is obtained, showing the existence of complicated singularities.

DOI: 10.1103/PhysRevE.95.012208

I. INTRODUCTION

Research on chaotic phenomena in nonlinear dynamical systems has been engaging attention and interest for many decades. From a mathematical point of view, dynamical chaos often is associated with the notion of a strange attractor, which is regarded as a nontrivial attractive limit set composed by unstable orbits and having the property of topological transitivity. Due to this definition one obtains two types of attractors: robust hyperbolic attractors and quasihyperbolic attractors [1] (also called Lorenz type attractors). Meanwhile nontrivial attractive sets have quite different natures for a majority of dynamical systems illustrating experimentally chaotic behaviors. Referred to as quasiattractors or nonhyperbolic attractors [2,3], they contain not only nontrivial hyperbolic sets, but also attractive periodic orbits.

Noise-induced escape from a strange attractor plays an extremely significant role in the theory of fluctuations and is of great importance for practical applications, including laser systems, neuron dynamics, and the control of migration in multistable systems [4–6]. However, solving such problems is a formidable task as a result of complicated structures of chaotic attractors and the ignorance of the way in which fluctuational trajectories break away. For small random perturbations, the Freidlin-Wentzell theory of large deviations [7] provides a proper framework to depict their effects on dynamics. Put simply, the theory builds on the fact that almost unlikely events, when they occur, do so with an overwhelming probability in the way that is least improbable. The mathematical treatment involves a set of dynamical equations providing extrema to certain action functionals in the path integral formulation of the stochastic process. The most probable escape path (or optimal path) gives rise to the absolute minimum to the action functional which characterizes the difficulty of the arrival at a given point along a separate path. The quantity of the action serves as the exponential rate of a stationary probability density in approximated Wentzel-Kramers-Brillouin (WKB) form in the weak noise limit [8]. As noise intensity tends to zero, these probabilities become exponentially small, but the rate of falling off is path dependent. It follows that for a given noise intensity the probability moving along the optimal path is exponentially larger than the ones along other paths.

However, limited work has been performed in terms of chaotic attractors. Anishchenko and co-workers [9,10] studied the noised-induced escape from a quasihyperbolic attractor in the Lorenz system, showing that there exists a unique escape path consisting of three parts and the role of noise in each part is different. Noise-induced escape from a nonhyperbolic chaotic attractor in a periodically excited nonlinear oscillator was considered by Luchinsky and Khovanov [11] via a statistical analysis of escape paths. According to Kraut and Grebogi [12], escape from a nonhyperbolic chaotic attractor starts at the primary homoclinic tangency [13] closest to the basin boundary. Their findings were substantiated in the discrete case of the Hénon and Ikeda map. Inspired by this, the authors [14] found a structure of hierarchical heteroclinic crossings of stable and unstable manifolds of saddle cycles, through which the noised-induced escape occurs. We concluded that it is this deterministic structure of manifolds that determines the mechanism of escape from nonhyperbolic attractors. Similar hierarchical structures were found by Silchenko *et al.* [15] when studying the escaping mechanism for systems having fractal basin boundaries. Nevertheless, we remark that the fractalities of boundaries [15] or manifolds [14] are far from the key part of the problem. According to Grebogi *et al.* [16], the parameter from smooth to fractal boundary metamorphosis coincides with the one at which the stable and unstable manifolds of the saddle cycle of period 1 are tangent, i.e., $\mu_{sf} = \mu_1^*$. As the parameter $\mu \to \mu_{sf}$, the structure of hierarchical heteroclinic crossings is being constructed by a sequence of saddle-node bifurcations with saddle cycles of higher and higher periods involved. Therefore, the escaping mechanism actually is provided by the structure of heteroclinic crossings which arises in both cases: smooth and fractal basin boundaries.

Another aspect of noise-induced escape is the pattern of fluctuational paths and corresponding singularities. Using the Hamiltonian formalism, one can obtain an auxiliary Hamiltonian system, whose trajectories emanating from a stable state trace out the unstable Lagrangian manifold. Even if Hamiltonian trajectories do not intersect in the Lagrangian manifold, the manifold may have complicated structures leading to intersections of their projections into the coordinate space. Consequently several fluctuational paths may arrive at

*czkillua@icloud.com
†Corresponding author: xbliu@nuaa.edu.cn

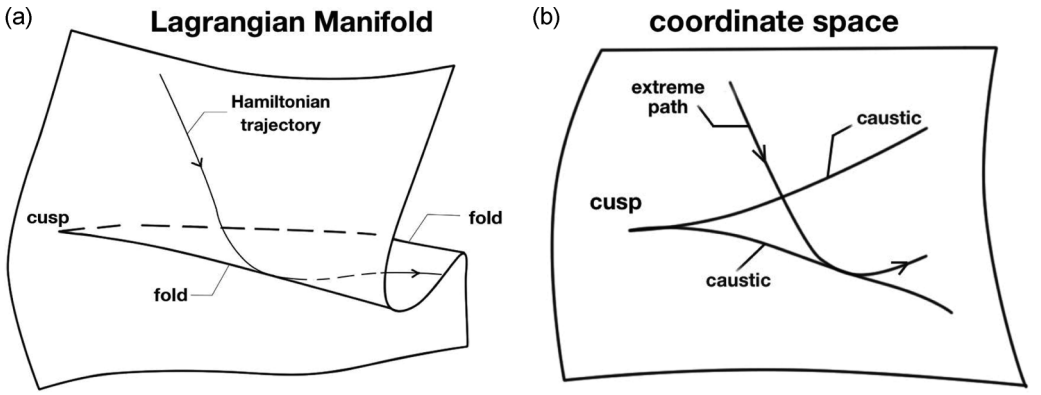

FIG. 1. (a) The Lagrangian manifold is traced out by trajectories of the auxiliary Hamiltonian system. The Lagrangian manifold has folds and cusps, and a trajectory on it is plotted by a curve with arrows. (b) Extreme paths are projections onto the coordinate space. The caustics are projections of folds in (a), and a trajectory going over the fold is described by an extreme path reflected by the caustic.

the same point, and patterns for nonequilibrium systems may have singular features, such as cusps and caustics [17,18]. They stem from complicated topological structures of the Lagrangian manifold, a schematic plot of which is given in Fig. 1 for illustration. As can be seen, each cusp gives rise to a pair of folds in the Lagrangian manifold, and their projections are caustics. When a Hamiltonian trajectory in the Lagrangian manifold goes over a fold, the corresponding fluctuational path in coordinate space, sometimes called an extreme path, is reflected by one of the caustics. However, little work has been performed for patterns from chaotic attractors due to the lack of awareness of the escaping mechanism.

The main purpose of this paper is to present a further study dealing with the subtle escaping modes and patterns of fluctuational paths from a nonhyperbolic chaotic attractor. The deviation amplifying effect of the primary homoclinic tangency is shown, and it demonstrates the rationality for choosing it as the initial point in our study. We found that exit from the domain of attraction of the nonhyperbolic attractor occurs through the saddle cycle of period 1 on the basin boundary. Furthermore, there mainly exist three ways for the trajectories to escape the saddle cycle: passing across it transversely, approaching it asymptotically, and being reflected back unsuccessfully. It is these subtle escaping behaviors that help to explain the complicated and nested structure of the action plot. Based on the structure of heteroclinic crossings, a subset of the pattern of fluctuational paths from the chaotic attractor is given, which shows a great deal of singularities, such as caustics and cusps. This paper is organized as follows. In Sec. II we formulate the problem. The Hamiltonian formalism is employed leading to an auxiliary dynamical system in Sec. III. More accurate results of the action plot are given in Sec. IV, and a detailed analysis is performed. Section V is contributed to the discussions on the patterns of fluctuational paths and the related singularities. Conclusions are drawn in Sec. VI.

II. FORMULATIONS

The periodically excited nonlinear oscillator in the presence of white noise was chosen as the model for investigation,

$$\begin{aligned} q_1 &= K_1[\mathbf{q}(t)] = q_2, \\ q_2 &= K_2[\mathbf{q}(t)] = -2\Gamma q_2 - \omega_0^2 q_1 - \beta q_1^2 - \gamma q_1^3 \\ &\quad + h\,\sin(\omega_f t) + \xi(t). \end{aligned} \tag{1}$$

Here q_1, q_2 are dynamical variables, and $\xi(t)$ is the Gaussian white noise such that $\langle \xi(t) \rangle = 0$, $\langle \xi(t)\xi(s) \rangle = D\delta(t-s)$. D is the noise intensity, and $\Gamma, \omega_0, \beta, \gamma, h$, and ω_f are parameters, which are chosen as $\Gamma = 0.025$, $\omega_0 = 0.597$, $\beta = 1$, $\gamma = 1$, $\omega_f = 1.005$, and $h = 0.145$ throughout this paper. Here Eq. (1) is a nonautonomous system due to the harmonic driving term keeping the system away from equilibrium. In order to make it autonomous, we obtain the following:

$$\begin{aligned} \dot{q}_1 &= K_1[\mathbf{q}(t)] = q_2, \\ \dot{q}_2 &= K_2[\mathbf{q}(t)] = -2\Gamma q_2 - \omega_0^2 q_1 - \beta q_1^2 - \gamma q_1^3 \\ &\quad + h\,\sin(q_3) + \xi(t), \\ \dot{q}_3 &= K_3[\mathbf{q}(t)] = \omega_f. \end{aligned} \tag{2}$$

The system (2) is three dimensional, but it is now autonomous. We remark that the state space of system (2) is $\mathbf{R}^1 \times \mathbf{R}^1 \times \mathbf{S}^1$.

Global analysis of the deterministic system was performed by the method of the generalized cell mapping with a digraph [19], and detailed discussions are given in Ref. [14]. To make this paper self-content, we show the domain of attraction of the nonhyperbolic chaotic attractor in Fig. 2(a) from which one can see its smooth boundary is formed by the stable manifold of the saddle cycle of period 1 (UC1 for short). Figure 2(b) is obtained by an iterative procedure capable of refining self-cycle sets of UC1, UC3, and a nonhyperbolic chaotic attractor to any degree of accuracy we desire. UC9 is found to locate in the vicinity of the attractor. The numbers in Fig. 2(b) are used to reveal the orders of iterations of these periodic cycles.

III. THE WKB APPROXIMATION

The WKB approximation $P(\mathbf{q}) \approx C(\mathbf{q})\exp[-S(\mathbf{q})/D]$ for $D \to 0$ then is employed to deduce the Hamiltonian system describing extreme fluctuational paths, where $P(\mathbf{q})$ is the

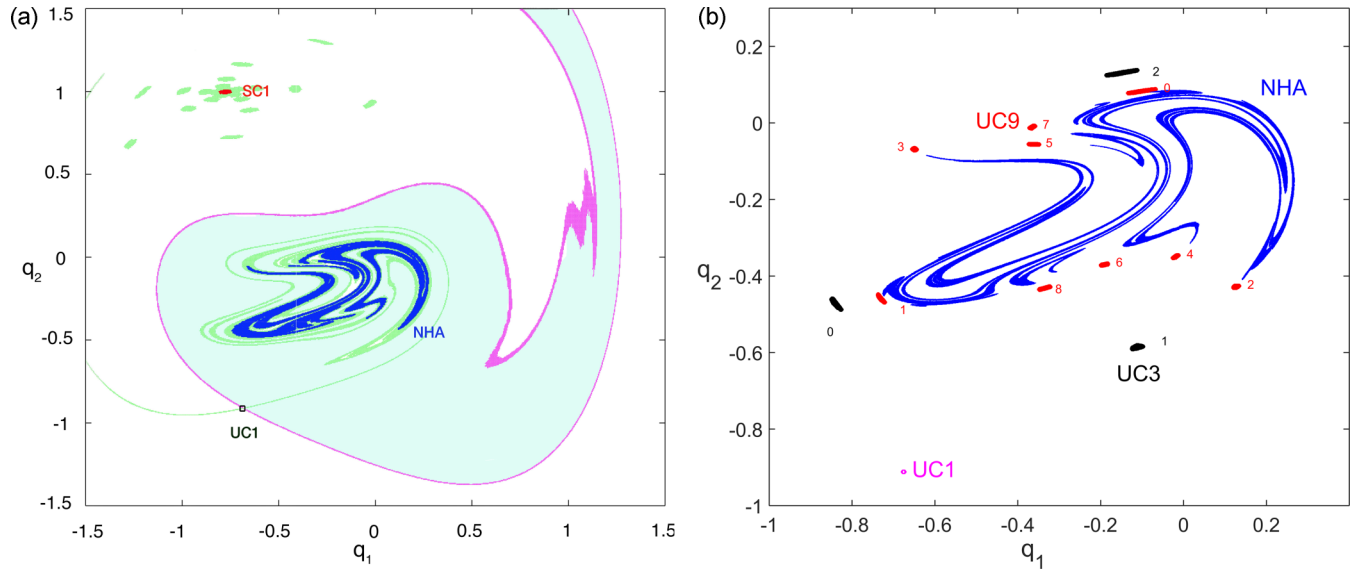

FIG. 2. Global results of (1) without noise in the Poincaré section $q_3 = 0 \pmod{2\pi}$. (a) The basin of attraction of the chaotic attractor indicated by the cyan shaded regions. The magenta curves are the stable manifolds of UC1, and the green curves are its unstable manifolds. (b) A local refinement of the region near the attractor indicated by the blue dots. The red dots denote the saddle cycle of period 9 (UC9 for short), and the black ones denote the saddle cycle of period 3 (UC3 for short). The magenta dots at the bottom represent UC1. The cell size is $0.000\,9375 \times 0.000\,9375$.

stationary probability density, $C(\mathbf{q})$ is a prefactor beyond the scope of this paper, and $S(\mathbf{q})$ is the action calculated along a certain trajectory to the terminal point $\mathbf{q}$. Through procedures given in the Appendix, we have the Wentzell-Freidlin Hamiltonian for (2) as follows:

$$H = \tfrac{1}{2}p_2^2 + p_1 q_2 + \left[-2\Gamma q_2 - \omega_0^2 q_1 - \beta q_1^2 - \gamma q_1^3 + h\sin(q_3)\right]p_2 + \omega_f p_3, \tag{3}$$

and the auxiliary Hamiltonian system,

$$\begin{aligned}
\dot{q}_1 &= \dot{q}_2,\\
\dot{q}_2 &= p_2 - 2\Gamma q_2 - \omega_0^2 q_1 - \beta q_1^2 - \gamma q_1^3 + h\sin(q_3),\\
\dot{q}_3 &= \omega_f,\\
\dot{p}_1 &= \left(\omega_0^2 + 2\beta q_1 + 3\gamma q_1^2\right)p_2,\\
\dot{p}_2 &= -p_1 + 2\Gamma p_2,\\
\dot{p}_3 &= -h\cos(q_3)p_2.
\end{aligned} \tag{4}$$

The Hamiltonian flow lies in a six-dimensional phase space spanned by the coordinate $\mathbf{q} = (q_1, q_2, q_3)$ and the momentum $\mathbf{p} = (p_1, p_2, p_3)$. In Sec. II we transformed system (1) into an autonomous one by adding q_3 in Eq. (2). It leads to an additional momentum p_3 in the Hamiltonian system (4). However, note that equations of q_1, q_2, p_1, p_2 in Eq. (4) do not contain p_3, thus it makes no difference to evolutions of extreme paths and related momenta, not to mention the action functional,

$$\begin{aligned}
S[\mathbf{q}(t)] &= \int_{t_0}^{t_f} dt\; L(\mathbf{q},\dot{\mathbf{q}}) = \int_{t_0}^{t_f} dt\; \frac{1}{2}(\dot{\mathbf{q}} - \mathbf{F})^T(\dot{\mathbf{q}} - \mathbf{F})\\
&= \int_{t_0}^{t_f} \frac{1}{2}p_2^2 dt,
\end{aligned} \tag{5}$$

where $\mathbf{F}$ denotes the deterministic vector field. Actually we performed this transformation to take advantage of the fact that a periodic oscillation of system (1) without noise is a closed curve of system (2) not intersecting itself in the phase space $\mathbf{R}^1 \times \mathbf{R}^1 \times \mathbf{S}^1$. In Sec. V where we obtain the pattern of fluctuational paths by choosing point 0 of UC9, the autonomous system (2) helps us to avoid calculations related to the specific form of the Poincaré map of the nonautonomous (1). Nevertheless, it has no influence on the action plot in Sec. IV due to the discussions above and Eq. (5).

IV. DETAILED DISCUSSIONS ON THE ESCAPE SCENARIO

The primary homoclinic tangency has been located by the algorithm proposed by Jaeger and Kantz [13] and selected as the initial point of escape paths. Subsequently the action plot was given, leading to the determination of the most probable escape path. Now let us discuss the action plot in more detail here, which is shown in Fig. 3(a).

In the vicinity of the primary homoclinic tangency, the escape trajectories can be parametrized by choosing their initial conditions on a small circle centered at the point. Some 10^6 initial points are uniformly distributed on a small circle with a radius of 10^{-5}. Thus the angular position is the parameter we use to trace out the set of escape trajectories on the unstable manifold. One may note that Fig. 3(a) appears different from that of Ref. [14] since the radius here is much smaller. The main concern there is the mechanism of escape, that is to say, the global minimum of the action plot but not its precise structure. However, a comparison between the optimal path corresponding to the global minimum of Fig. 3(a) and the statistical results obtained by the concept of prehistory probability distributions [20] illustrates rather good agreement, see Figs. 3(b)–3(d). We omit detailed descriptions on statistical

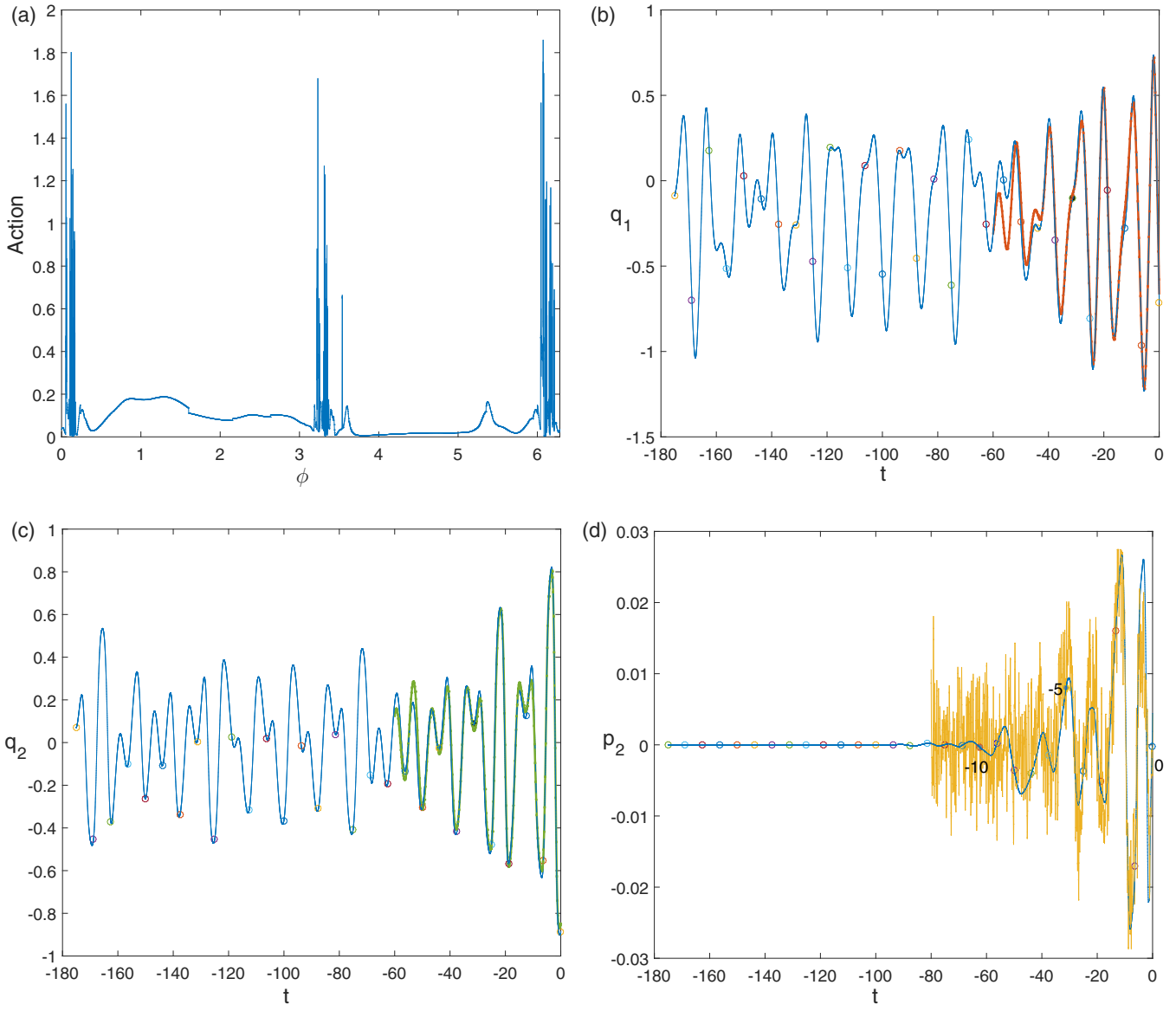

FIG. 3. (a) The action plot for our system. The x axis is the angular position to parametrize the escape trajectories, ranging from $[0,2\pi)$. Some 10^6 points are taken in this range. (b)–(d) Comparisons between the optimal path of the action plot (blue solid lines) and the result of statistical analysis (red, green, and yellow lines). (b) q_1. (c) q_2. (d) p_2.

analysis here, and one can refer to Ref. [14] for more details. Moreover, we remark that the precise structure of the action plot does not change anymore when the radius is below a certain threshold, ensuring the validity of this method.

Two implications can be obtained from Fig. 3(d). One is that decreasing the radius of the circle is essentially increasing the time length of the "deterministic" dynamics during which the fluctuational force is nearly zero. It is apparent since more time is needed to deviate from the attractor for those points closer to the primary homoclinic tangency which belongs to the nonhyperbolic chaotic attractor. Therefore it makes little difference to the action plot by reducing the radius below a certain threshold.

The other one is that the optimal force p_2 remains approximately equal to zero until some instant of time, which is indicated by -10 in Fig. 3(d), begins to "wiggle." The optimal path is plotted in the section $q_3 = 0 \,(\mathrm{mod}\, 2\pi)$ with each intersection point labeled with a number, see Fig. 4. One can see that the point labeled -10 in green locates closely to the primary homoclinic tangency, denoted by a black square. Indeed, we have not yet given any straightforward evidence supporting our choice taking the primary homoclinic tangency as the beginning of the escape, except our faith in related Refs. [12,13,21,22]. However, we are convinced that Fig. 3(d) together with Fig. 4 provide what we seek. Recalling Eq. (5) we can see that p_2 actually measures the divergence of the optimal path from deterministic dynamics. To be more specific, starting from a point sufficiently close to the primary homoclinic tangency, the optimal path moves very close to the deterministic dynamics ($p_2 \approx 0$) with deviations sufficiently small at first. Nevertheless, they are still accumulating until sometime when the optimal path moves back to the vicinity

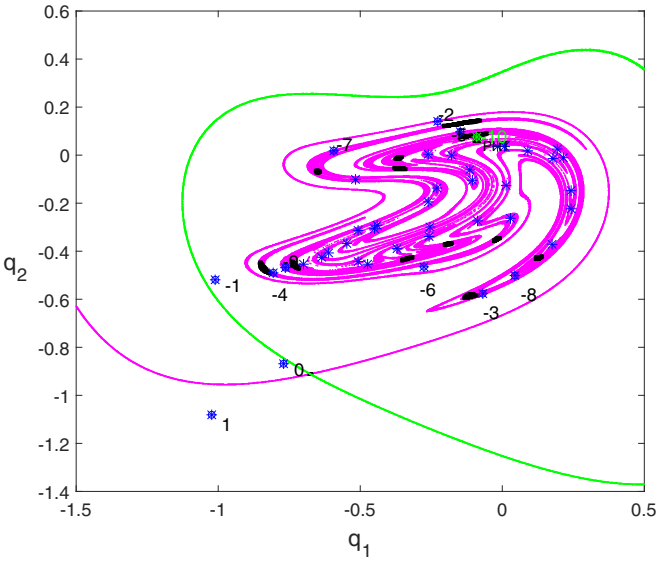

FIG. 4. The optimal path in the section $q_3 = 0 \pmod{2\pi}$, plotted by blue stars with numbers to indicate the orders. The green lines are the stable manifolds of UC1, and the magenta lines are one branch of the unstable manifold of UC1 (left) and the unstable manifold of UC9 (right), respectively. The label -10 corresponds to the same point in Fig. 3(d).

of the primary homoclinic tangency. At this moment, labeled -10 in Figs. 3(d) and 4, deviations are no longer neglectable and further amplified by forward evolutions. The sequential amplifications then are delineated by the optimal force p_2 which begins to fluctuate dramatically. This landscape is consistent with both our results and the pioneering works on homoclinic tangencies [13,23].

Now let us turn to study some subtle details of the action plot. Intuitively, there are two types of escape trajectories. The first type is that they can cross the boundary of the domain of attraction with nonzero momenta and then move further to reach the domain of attraction of another stable state. The second one corresponds to a different scene: They first move towards the basin boundary, but their momenta are not sufficient to escape. Then they are reflected from the boundary back to the interior of the original basin, fluctuating around the attractor again and preparing for the next trial. Since the basin boundary is a stable manifold of UC1, between the two types of escape paths is the third one: heteroclinic trajectories which approach the saddle cycle UC1 lying on the boundary with momenta tending to zeros. In other words, these heteroclinic trajectories lie in the intersections of the unstable manifold of the attractor with the stable manifold of UC1.

However, the actions of these types of escape paths are totally different. Consider a path that is a perturbation of a heteroclinic trajectory with its momentum slightly bigger than that of the heteroclinic trajectory. Consequently this path crosses the boundary and pierces the cycle UC1 with a residual momentum. Thus the action of this path is also slightly larger than that of the heteroclinic trajectory, implying a continuous change in the parameters of the action plot. On the other hand, if the momentum of the perturbed path is a bit smaller than the heteroclinic trajectory, it will be reflected back. During its second attempt to escape its momentum will become significantly nonzero again, resulting in a highly larger action than that in its last run. This in turn gives rise to a discontinuous change in the action plot, and it follows that the discontinuities correspond to heteroclinic trajectories. The lowest-cost heteroclinic trajectory is the optimal one [24].

It can be observed from Fig. 5(a) that the action plot has a rather complicated structure composed of narrow "hills" and very sharp "peaks." At the edges of the hills, discontinuities, i.e., local minima of the action, are present. It follows from the discussions above that each discontinuity, say arrow 1 in Fig. 5(a), corresponds to a heteroclinic trajectory which is plotted in Fig. 5(b) with thin lines. The circles and the yellow triangle represent the intersections of the escape trajectory and UC1 with the section $q_3 = 0 \pmod{2\pi}$, respectively. We only display the last few periods of the path before its final escape, which takes place through UC1 in an asymptotic way. In Fig. 5(c) another escape path associated with arrow 2 in Fig. 5(a) is shown. It crosses UC1 with a nonzero angle (or transversely) and thus pierces the boundary with residual momenta. Note that the parameter can be changed continuously from arrow 2 to arrow 1. The trajectories in the peaks have significantly larger costs, say arrow 3 in Fig. 5(a). They are paths that have been reflected back and experienced an unsuccessful attempt as shown in Fig. 5(d). Nested peaks of the action plot imply a sequence of reflections from UC1 before the final successful escape. This explains the complicated and nested structure of the action plot. Finally we end this section by pointing out that strict heteroclinic trajectories can hardly be determined but can only be approximated by numerical methods since infinite time is needed for them to approach the saddle cycle.

V. HEURISTIC DISCUSSIONS ON PATTERNS AND SINGULARITIES

Singularities of the pattern of fluctuational paths are obtained and studied for various systems with regular attractors, such as equilibrium points [25,26] and limit cycles [27,28]. However, little work has been performed for escapes from chaotic attractors as general mechanisms of such escapes are usually unknown. However, based on the hierarchical heteroclinic structures we found [14], some previously unsolved problem encounters a rare glimmer of hope.

It is found that escape occurs through a hierarchical sequence of crossings between stable and unstable manifolds of saddle cycles, manifesting itself as a series of "jumps" from one unstable manifold to another, see Fig. 10 in Ref. [14]. It leads us to conclude that the Lagrangian manifold emanating from the attractor contains this hierarchical heteroclinic structure as its part. If we consider the unstable manifold of UC9 in the configuration of Hamiltonian system (10), we can trace out a subset of the Lagrangian manifold, giving a glimpse of its mystery and complexity. Therefore in the following we choose point 0 of UC9, see Fig. 2(b), as the initial point where the subset of the Lagrangian manifold emanates.

In Fig. 6 patterns of fluctuational paths are presented for which we choose point 0 of UC9 as the start. They are solutions of Eq. (4) through direct integrations with a family of parametrized initial conditions [24] centered at point 0 and

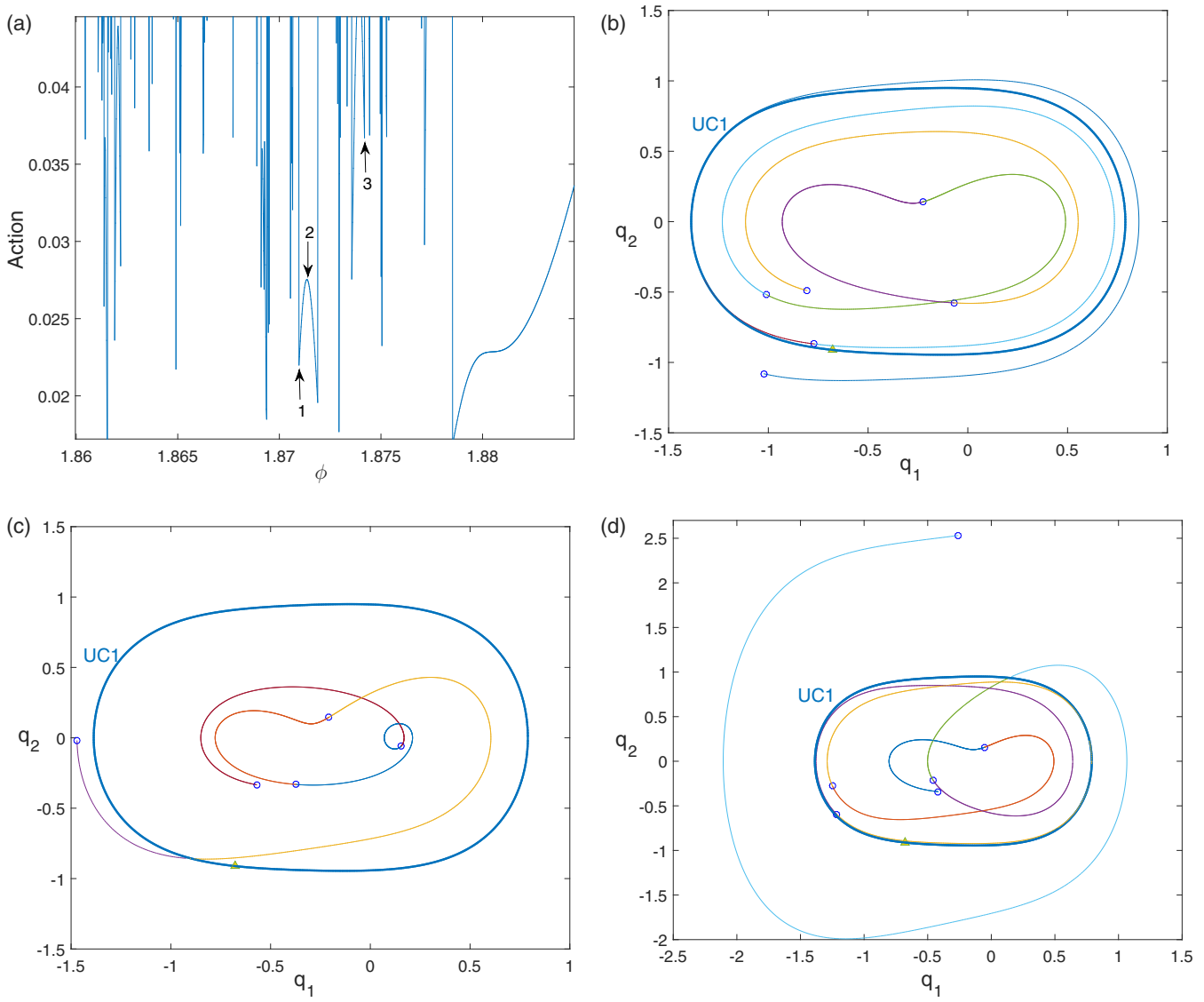

FIG. 5. (a) A local amplification of the action plot. Finer and nested structures are evident, and infinite many local minima between each pair of peaks can be seen. (b) Escape path corresponding to arrow 1 in (a) where a discontinuity is present. (c) Escape path corresponding to arrow 2 in (a). (d) Escape path corresponding to arrow 3 in (a).

uniformly located in its unstable eigenspace. Briefly speaking, by computing the Jacobian matrix of system (4) at point 0 one can give the relations between the momenta (p_1, p_2, p_3) and the coordinates (q_1, q_2, q_3). We omit the tedious but standard computation process, and one can refer to Ref. [24] for details. Only the first component $q_1(t)$ is presented as a demonstration here. One can see that the pattern has intricate and complex structures with several cusps and their own caustics. It should be clarified that the entire pattern which originates from the chaotic attractor must have more complicated structures than Fig. 6. However, how to delineate the whole unstable Lagrangian manifold of a strange attractor having fractal dimensions remains for a further study.

All fluctuational paths passing through UC1 are plotted by the cyan dotted lines in Fig. 7(a) with the terminating point marked by an arrow. The green dashed line, corresponding to the optimal path obtained through the action plot, is compared with the statistical result of Fig. 3, which is represented by a solid red line. Picking them out and omitting all other irrelevant paths we obtain Fig. 7(b) with the legend inside listing actions calculated along these paths. It is evident that actions related to the optimal paths, the solid red line, and the dashed green line, are lowest, compared with others. The values of the actions of optimal paths differ only by the order of 10^{-4} within a permissible range.

VI. CONCLUSIONS

In this paper we studied the noise-induced escape from a nonhyperbolic chaotic attractor of a periodically excited nonlinear oscillator. The primary homoclinic tangency is found to amplify deviations when the escaping trajectory returns to its close vicinity, giving rise to dramatic fluctuations of the optimal force. Its absolute value measures the divergence of the escaping trajectory from the deterministic motion, and the first occurrence of values bounded away from zero

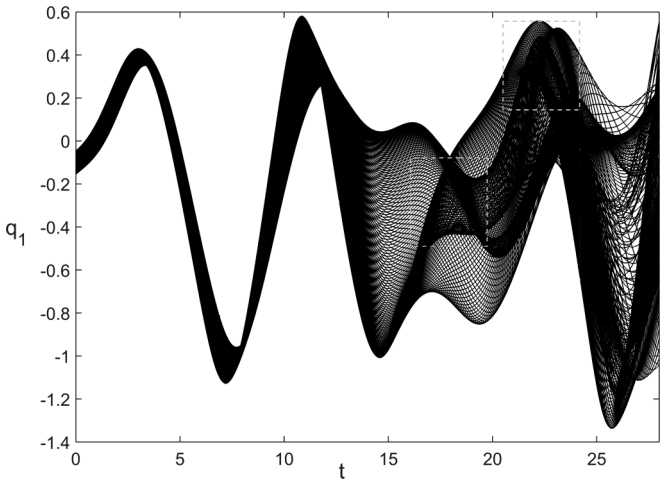

FIG. 6. Patterns of the fluctuational paths of (4), the initial point of which is chosen as point 0 of UC9. The dashed squares inside indicate where singularities exist.

marks the moment when the noise works and escape starts. It unambiguously supports us to choose the primary homoclinic tangency as the initial point of the escaping process.

We gave a detailed explanation about the complicated and nested structure of the action plot by exploring concrete modes that escaping trajectories possibly have to pass across the

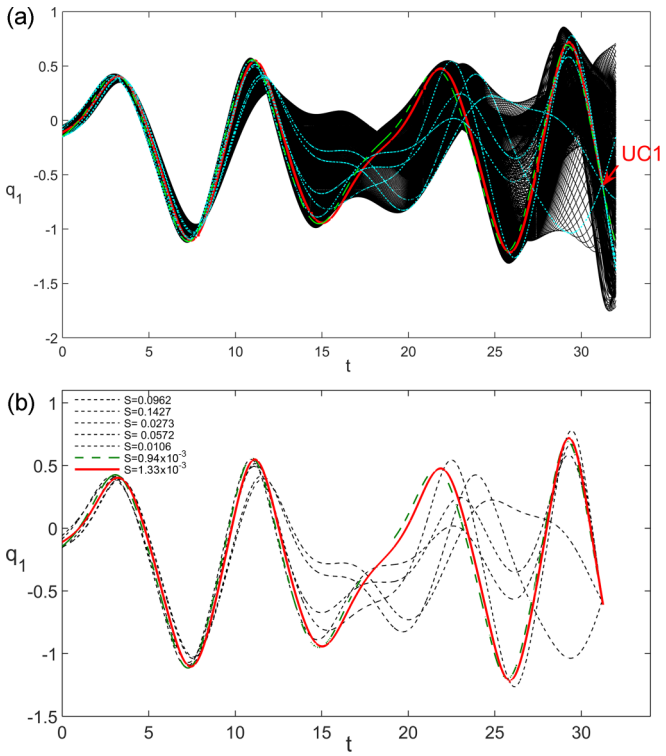

FIG. 7. (a) Fluctuational paths passing through UC1 are plotted with the cyan dotted curves. The red solid curve is obtained by statistical analysis in Fig. 3, and the green dashed curve is the optimal path. (b) Actions calculated along various paths. The minimum is taken by the optimal path, corresponding to the red solid line and the green dashed line.

saddle cycle lying on the basin boundary. They may pierce the cycle transversely with residual momentum, approach the cycle asymptotically with momentum tending to zero, and be reflected back with insufficient momentum after an unsuccessful attempt. It turns out that heteroclinic trajectories correspond to local extrema of the action plot and the most probable one has the global minimum action.

The escaping structure of heteroclinic crossings is also demonstrated in this paper. Based on this mechanism we can obtain the pattern of fluctuational paths escaping from the nonhyperbolic attractor. Even if only a subset of the pattern is obtained, it still shows sophisticated structures and singularities, embedded one in another. We found multiple extreme trajectories fluctuating to the saddle cycle of period 1 (i.e., UC1) and calculated the actions along each of them. They show multivaluedness and the most probable trajectory has the lowest action.

Before the end we remark that a complete study of the singular features of the pattern, or even of the topological structures of the Lagrangian manifold from a chaotic attractor, calls for further studies on the general mechanism of their inner formations *per se*. Due to this hierarchical sequence of crossings between stable and unstable manifolds of saddle cycles, we are convinced that escapes from nonhyperbolic chaotic attractors, having some stable periodic orbits of extremely long periods within their fractal structures [22], are deeply connected with saddle cycles resulting from the sequence of saddle-node bifurcations. Thus in this sense choosing point 0 of UC9 as a "reference point" of the pattern of fluctuational paths is somewhat reasonable and can yet be regarded as an alternative compromise at present.

ACKNOWLEDGMENTS

This research was supported by the National Natural Science Foundation of China (Grants No. 11472126 and No. 11232007) and the Project Funded by the Priority Academic Program Development of Jiangsu Higher Education Institutions (PAPD). The Research Fund of State Key Laboratory of Mechanics and Control of Mechanical Structures (Nanjing University of Aeronautics and Astronautics) (Grant No. MCMS-0116G01).

APPENDIX: THE DERIVATION OF THE HAMILTONIAN SYSTEM

If the noise intensity D is small, the system spends most of the time fluctuating about the attractor, only occasionally far away from it (of scale $\gg \sqrt{D}$). Occasionally, escape from the domain of attraction could occur. When it does occur, escape follows a unique optimal trajectory with an overwhelming probability, seemingly in an almost deterministic way. To determine the optimal trajectory, we must turn to investigate the asymptotic solution of the Fokker-Planck equation as $D \to 0$. In the limit of weak noise intensity D one can seek an approximate solution in an eikonal or WKB form

$$P(\mathbf{q}) \sim C(\mathbf{q})\exp\left[-\frac{S(\mathbf{q})}{D}\right], \tag{A1}$$

with $C(\mathbf{q})$ as a prefactor not investigated in this paper and $S(\mathbf{q})$ as the "activation energy" of fluctuations to the vicinity of the

point $\mathbf{q}$ in the state space. $S(\mathbf{q})$ is also called the quasipotential or nonequilibrium potential.

Substituting Eq. (A1) into the Fokker-Planck equation and keeping only the terms of lowest order in D, we obtain the Hamilton-Jacobi equation for $S(\mathbf{q})$,

$$H(\mathbf{q},\mathbf{p}) \equiv \mathbf{K}(\mathbf{q}) \cdot \mathbf{p} + \frac{1}{2}\mathbf{p}^T \mathbf{Q}\mathbf{p} = 0, \qquad \mathbf{p} \equiv \frac{\partial S}{\partial \mathbf{q}}, \tag{A2}$$

where the matrix $\mathbf{Q} = \mathrm{diag}(0,1,0)$ and $\mathbf{K}$ corresponds to the deterministic vector field in Eq. (1). To solve the Hamilton-Jacobi equation (A2) one can employ the method of characteristics, arriving at the following equations:

$$\frac{d\mathbf{q}}{dt} = \frac{\partial H}{\partial \mathbf{p}} = \mathbf{K}(\mathbf{q}) + \mathbf{Q}\mathbf{p}, \tag{A3}$$

$$\frac{d\mathbf{p}}{dt} = -\frac{\partial H}{\partial \mathbf{q}} = -\left[\frac{\partial \mathbf{K}(\mathbf{q})}{\partial \mathbf{q}}\right]^T \mathbf{p}. \tag{A4}$$

Note that Eqs. (A3) and (A4) lead to an auxiliary Hamiltonian dynamical system with the Wentzell-Freidlin Hamiltonian $H(\mathbf{q},\mathbf{p})$. From this point of view $S(\mathbf{q})$ can be interpreted as the classical action at zero energy [18].

Solutions of Eqs. (A3) and (A4) describe trajectories yielding extreme values of the cost functional of the form

$$\mathrm{S}[\mathbf{q}(t)] = \frac{1}{2}\int_{t_0}^{t_f} \xi^2(t)dt, \tag{A5}$$

with $\mathbf{q}(t)$ being a certain trajectory driven by the corresponding realization of $\xi(t)$ and satisfying $\mathbf{q}(t_0) = \mathbf{q}_0$ and $\mathbf{q}(t_f) = \mathbf{q}_f$. Since using (2) the cost functional (A5) can be transformed into an action functional,

$$S[\mathbf{q}(\mathrm{t})] = \int_{t_0}^{t_f} dt\ L(\mathbf{q},\dot{\mathbf{q}}), \quad L(\mathbf{q},\dot{\mathbf{q}}) = \frac{1}{2}(\dot{\mathbf{q}} - \mathbf{K})^T(\dot{\mathbf{q}} - \mathbf{K}). \tag{A6}$$

This has the form of a Lagrangian L for a classical mechanical system. As $D \to 0$, these path integrals (A6) can be evaluated by means of the steepest descents, and the paths dominating the integrals are the ones giving rise to $\delta S/\delta x = 0$. This results in a Euler-Poisson equation for extreme paths, which is a second-order nonlinear partial differential equation, and it can be converted into $2n$ first-order ordinary differential equations (A3) and (A4). In other words, the action $S(\mathbf{q})$ mentioned above is just given by the variational problem of (A6). Thus we have the Wentzell-Freidlin Hamiltonian for (2) as follows:

$$H = \frac{1}{2}p_2^2 + p_1 q_2 + \big[-2\Gamma q_2 - \omega_0^2 q_1 - \beta q_1^2 - \gamma q_1^3 + h\sin(q_3)\big]p_2 + \omega_f p_3, \tag{A7}$$

and the auxiliary Hamiltonian system,

$$\begin{aligned}
&\dot{q}_1 = \dot{q}_2, \quad \dot{q}_2 = p_2 - 2\Gamma q_2 - \omega_0^2 q_1 - \beta q_1^2 - \gamma q_1^3 + h\sin(q_3),\\
&\dot{q}_3 = \omega_f,\\
&\dot{p}_1 = \left(\omega_0^2 + 2\beta q_1 + 3\gamma q_1^2\right)p_2, \quad \dot{p}_2 = -p_1 + 2\Gamma p_2,\\
&\dot{p}_3 = -h\cos(q_3)p_2.
\end{aligned} \tag{A8}$$

[1] V. S. Anishchenko and G. I. Strelkova, Discrete Dyn. Nat. Soc. **2**, 53 (1998).
[2] L. Shil'nikov, J. Circuit Syst. Comp. **3**, 1 (1993).
[3] V. Anishchenko, A. Kopeikin, J. Kurths, T. Vadivasova, and G. Strelkova, Phys. Lett. A **270**, 301 (2000).
[4] R. L. Kautz, Rep. Prog. Phys. **59**, 935 (1996).
[5] R. D. Astumian and I. Derényi, Eur. Biophys. J. **27**, 474 (1998).
[6] E. A. Jackson, Chaos **7**, 550 (1997).
[7] M. I. Freidlin and A. D. Wentzell, *Random Perturbations of Dynamical Systems*, 3rd ed. (Springer-Verlag, Berlin, Heidelberg, 2012).
[8] P. Grassberger, J. Phys. A **22**, 3283 (1989).
[9] V. S. Anishchenko, I. A. Khovanov, N. A. Khovanova, D. G. Luchinsky, and P. V. E. McClintock, Fluctuation Noise Lett. **01**, L27 (2001).
[10] V. S. Anishchenko, D. G. Luchinsky, P. V. E. McClintock, I. A. Khovanov, and N. A. Khovanova, J. Exp. Theor. Phys. **94**, 821 (2002).
[11] D. G. Luchinsky and I. A. Khovanov, JETP Lett. **69**, 825 (1999).
[12] S. Kraut and C. Grebogi, Phys. Rev. Lett. **92**, 234101 (2004).
[13] L. Jaeger and H. Kantz, Physica D **105**, 79 (1997).
[14] Z. Chen, Y. Li, and X. Liu, Chaos **26**, 063112 (2016).
[15] A. N. Silchenko, S. Beri, D. G. Luchinsky, and P. V. E. McClintock, Phys. Rev. E **71**, 046203 (2005).
[16] C. Grebogi, E. Ott, and J. A. Yorke, Physica D **24**, 243 (1987).
[17] M. I. Dykman, M. M. Millonas, and V. N. Smelyanskiy, Phys. Lett. A **195**, 53 (1994).
[18] M. I. Dykman, D. G. Luchinsky, P. V. E. McClintock, and V. N. Smelyanskiy, Phys. Rev. Lett. **77**, 5229 (1996).
[19] C. S. Hsu, Int. J. Bifurcation Chaos Appl. Sci. Eng. **5**, 1085 (1995).
[20] M. I. Dykman, P. V. E. McClintock, V. N. Smelyanski, N. D. Stein, and N. G. Stocks, Phys. Rev. Lett. **68**, 2718 (1992).
[21] C. G. Schroer, E. Ott, and J. A. Yorke, Phys. Rev. Lett. **81**, 1397 (1998).
[22] S. Gonchenko, L. Shil'nikov, and D. Turaev, Comput. Math. Appl. **34**, 195 (1997).
[23] M. Diestelhorst, R. Hegger, L. Jaeger, H. Kantz, and R.-P. Kapsch, Phys. Rev. Lett. **82**, 2274 (1999).
[24] S. Beri, R. Mannella, D. G. Luchinsky, A. N. Silchenko, and P. V. E. McClintock, Phys. Rev. E **72**, 036131 (2005).
[25] D. G. Luchinsky, R. S. Maier, R. Mannella, P. V. E. McClintock, and D. L. Stein, Phys. Rev. Lett. **79**, 3109 (1997).
[26] R. S. Maier and D. L. Stein, J. Stat. Phys. **83**, 291 (1995).
[27] V. N. Smelyanskiy, M. I. Dykman, and R. S. Maier, Phys. Rev. E **55**, 2369 (1997).
[28] Z. Chen and X. Liu, Phys. Lett. A **380**, 1953 (2016).